

## Isotopic fragmentation distribution of $^{129}\text{Xe}$ on $^{90}\text{Zr}$ and $^{197}\text{Au}$ targets at intermediate energy

J. Feng, W. Q. Shen, and Y. G. Ma

*Institute of Nuclear Research, Academia Sinica, Shanghai 201 800, China*

W. L. Zhan, Y. T. Zhu, and Z. Y. Guo

*Institute of Modern Physics, Academia Sinica, Lanzhou 730 000, China*

L. Tassun-Got, C. Stephan, A. Gillibert, Y. Schutz, P. Juzun, and W. Mittig

*GANIL, Boite Postal 5027, Caen, France*

(Received 25 April 1994)

The isotopic distributions of projectile fragmentation have been measured for the reaction of 44 MeV/nucleon  $^{129}\text{Xe}$  on  $^{90}\text{Zr}$  and  $^{197}\text{Au}$  targets. The systematics of the production cross sections are discussed via some macroscopic models.

PACS number(s): 25.70.Mn, 24.10.-i

The investigation of the isotopic fragmentation distribution of heavy-ion peripheral collisions can provide not only a valuable insight into the nature of the reaction mechanism but also an important reference for searching for new isotopes and for developing radioactive nuclear beams. The formation of projectilelike fragmentation products in peripheral heavy-ion collisions at intermediate energies has been studied both experimentally [1-8] and theoretically [9,10]. Some measurements for projectiles (up to  $^{86}\text{Kr}$ ) on various targets at intermediate energies have been reported [1-8], but the detailed explanation of some aspects of the observed phenomena is still in an unsatisfactory state. In this energy range the production mechanism for fragments is not yet well understood. Why the abrasion-ablation model, which can reproduce the experimental isotopic distribution of a  $^{40}\text{Ar}$  induced reaction, cannot explain the  $^{86}\text{Kr}$  results is still an open question. Furthermore, there are only few experimental data on fragmentation isotopic distributions for heavy projectile-induced reactions at intermediate energies. It will be very useful to have more experimental data of isotopic fragmentation distributions with heavier projectiles for systematic studies of the behavior of fragmentation and for searches for new heavy exotic nuclei such as  $^{100}\text{Sn}$ , which may represent the limit to nuclear structure studies of the  $N = Z$  nuclei.

Following this idea, in this paper we report the experimental isotopic distributions of the reaction induced by 44 MeV/nucleon  $^{129}\text{Xe}$  beam on various targets. The comparisons with some model predications are also discussed.

In the present study, a beam of 44 MeV/nucleon  $^{129}\text{Xe}$  ions delivered by the GANIL cyclotrons was used to bombard a  $^{90}\text{Zr}$  (1.13 mg/cm<sup>2</sup>) and a  $^{197}\text{Au}$  (0.9 mg/cm<sup>2</sup>) target, respectively. Both targets were mounted at the intermediate focal plane of the SPEG spectrometer [11]. They were chosen because the projectile mass was between the two target masses so that different kinematics and target effects for producing higher yields of fragment could be studied. Beam intensities on the targets were typically 10 nA. The center angle of the SPEG was set

at 3 degrees with a horizontal open angle of  $\pm 2$  degrees. The dispersion and the momentum acceptance  $\Delta P/P$  of the magnetic spectrometer were set to be 8 cm per percent and  $\pm 3\%$ , respectively. Two drift chambers for measuring the horizontal and vertical positions of reaction products were put in front of and behind the focal plane, respectively, so that it could give a precise magnetic rigidity. The time-of-flight (TOF) start signal was provided by a parallel plate avalanche counter, which was located at the focal plane. The TOF stop signal was derived from the radio-frequency signal of the cyclotron. The flight path length was 14.2 m. The focal plane detector was composed of a Bragg detector and two ionization chambers, which could give the energy, range, and  $\Delta E$  information. The veto detector was a plastic scintillator detector.

Combining the magnetic spectrometry with the energy-loss and range measurements in the Bragg detector made it possible to identify reaction products unambiguously as described in Ref. [12]. Figure 1(a) shows the ion charge number  $Z$  spectra of 44 MeV/nucleon  $^{129}\text{Xe}$  on the  $^{90}\text{Zr}$  target, which are obtained by the energy-range particle identification method. The elements from Xe to Kr can be clearly distinguished. Fragments with a charge number larger than the projectile's are observed. This can be explained as the result of nucleon transfer from the target to the projectile. From the figure, some interesting phenomena can be observed, which we cannot explain at present: the yields of  $Z = 46$  and  $48$  isotopes are smaller than their odd- $Z$  neighbors' in this reaction. This is an intricate effect, since the detailed structure of the isotope distribution depends on the competition of several things, such as the distance from the stability line and from the projectile, the nuclear structure effects, etc. A detailed explanation should be very useful in understanding this reaction. Figure 1(b) is the ionic charge state distribution for a given atomic number. Four to five charge states are measured at one magnetic rigidity  $B\rho$ . The resolution of the charge state  $Q$  is mainly decided by the energy resolution because of the high resolution of the magnetic spectrometer and the precise measurement of

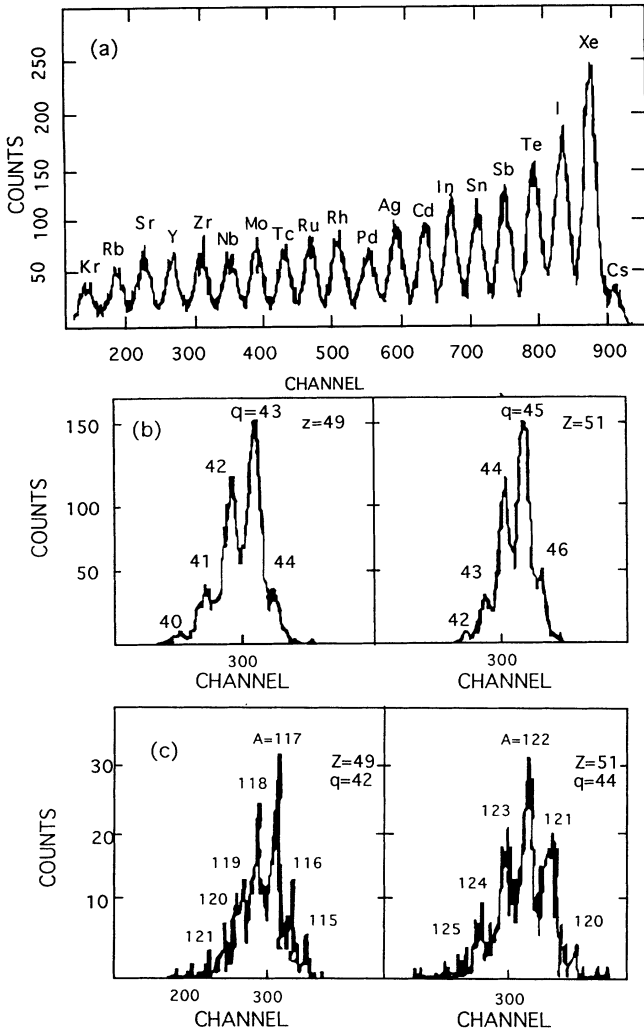


FIG. 1. The particle identification spectra of fragments produced by 44 MeV/nucleon  $^{129}\text{Xe}$  on  $^{90}\text{Zr}$  targets. (a) The atomic number  $Z$  spectrum. (b) The spectra of particles versus charge state for two values of  $Z$ . (c) The mass number  $A$  spectrum.

the TOF. Figure 1(c) is the mass spectra. In order to improve the mass resolution several cuts have been applied to these data including charge cuts and charge-state cuts of 0.2%, respectively. Because of the limited acceptance some charge state and energy spectra cannot be measured. These have been compensated for by software correction. The errors caused by these corrections are around several percent.

The measured isotopic production cross sections are given in Fig. 2, in which triangles and solid dots represent the reaction on  $^{90}\text{Zr}$  and  $^{197}\text{Au}$  targets, respectively. The experimental isotopic distributions of Cd and Sn are almost centered near the valley of stability (shown as arrows). The Ag and In isotopic distributions are also centered not far from the stability line. This phenomenon is unexpected in that the heavier projectile should produce nuclei near the drip line because of the geometry of the abrasion mechanism and the low excitation energy deposited in the prefragments according to the systematics of  $^{40}\text{Ar}$  at 44 MeV/nucleon. It indicates that the reaction process appears to be very dissipative and leads to the formation of highly excited prefragments. Quantitatively, a better understanding of this process is very important to optimize the experimental conditions for the purposes. In the case of searching for  $^{100}\text{Sn}$ , it is better to use higher incident energy to reach the pure fragmentation regime, which has a higher cross section. The peaks of the isotopic distributions for these two systems are almost located in the same position. This indicates that the target is a spectator, as in the high-energy projectile fragmentation. We also can see that the lighter the target mass the larger the cross section. But the difference between them is small. This evolution confirms that the kinematical focusing effects play a role in heavy-ion peripheral collisions at intermediate energy.

In Fig. 3 the comparison is made to different model calculations. For systematics, the isotopic distribution of 44 MeV/nucleon  $^{40}\text{Ar}+^{181}\text{Ta}$  reaction from Ref. [6] is also given. The results of a calculation by a fragmentation model, which is based on the abrasion-ablation pic-

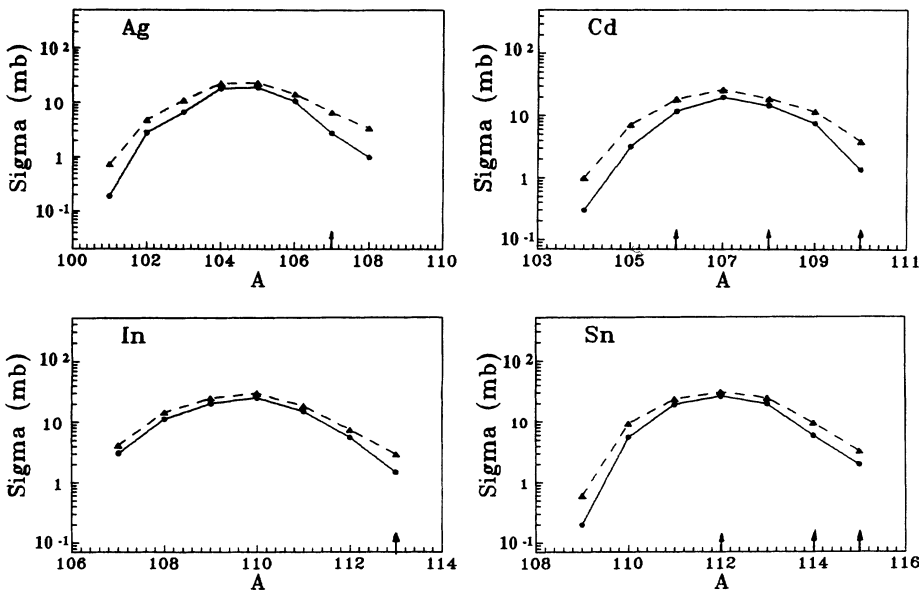


FIG. 2. The isotopic distribution of fragments of 44 MeV/nucleon  $^{129}\text{Xe}$  on  $^{90}\text{Zr}$  and  $^{197}\text{Au}$  targets. The curves are just for guiding the eye (for more details, see text).

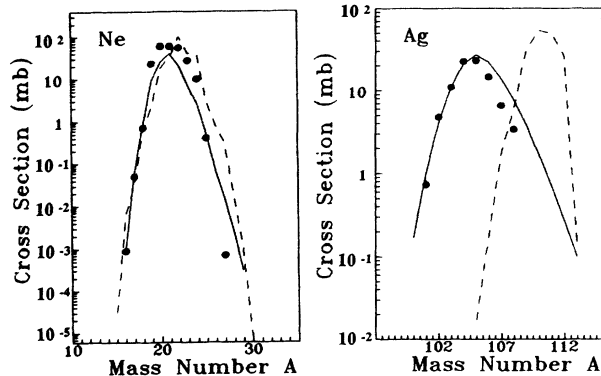


FIG. 3. Comparison of the isotopic distribution with model calculations. The solid dots represent experimental results. The curves represent model calculation. The neon isotopic distribution is from 44 MeV/nucleon  $^{40}\text{Ar}+^{181}\text{Ta}$  reaction [6]. The silver isotopic distribution is from our experimental result of 44 MeV/nucleon  $^{129}\text{Xe}+^{90}\text{Zr}$  reaction (for more details, see the text).

ture and incorporates the giant dipole resonance and a deexcitation process [13–15], is shown as dashed curves in Fig. 3. The dots represent the experimental results. This calculation considers that the dominant reaction mechanism around the Fermi energy range is similar to a pure fragmentation process at high energies and neglects the dissipative phenomena existing at intermediate energies. We can see that both the peak and width of the isotopic distribution of the 44 MeV/nucleon  $^{40}\text{Ar}$  induced reaction can be reproduced very well. But it is completely different in the 44 MeV/nucleon  $^{129}\text{Xe}$  case. The difference of the peak position between the experimental and calculated results is about 6 amu. A possible explanation is that in the 44 MeV/nucleon  $^{129}\text{Xe}$  induced reaction, a large amount of energy is dissipated in the primary fragments and the reaction products will move in the direction of the  $\beta$ -stability line by evaporating more nucleons and particles.

Sümmerer *et al.* developed a new parametrization for calculating cross section of fragments for projectiles with mass larger than approximately  $A = 40$  for high-energy heavy-ion reactions [16]. They considered the influence of the projectile  $N/Z$  ratio on the fragmentation in that calculation and used a modified parametrization of the proton excess, which drastically effects the cross section of heavy fragments. Their parametrization calculation can reproduce about 700 experimental fragment cross sections within a factor of 2. In order to see if there is a substantial difference at intermediate bombarding

energies, a comparison is made with our experimental results. The solid curve in Fig. 3 is the calculated result of Sümmerer's parametrization formula. Surprisingly, we can see that this simple parametrization can fit the experimental results fairly well for both reactions. The neutron deficient side is in good agreement for the Xe fragment. But a large deviation for the neutron-rich Xe fragments is observed. This may indicate that an inherent overestimation in Sümmerer's parametrization calculation exists for the widths of isobaric chains close to the projectile. For reproducing the fragment cross section for a heavier fragment, a parameter  $\Delta$ , which is a shift of the centroid of the charge distribution toward the  $\beta$  stability with decreasing mass loss from the projectile, has to be introduced into the calculation [16].

In the comparison with the fragmentation of the heavier ( $^{129}\text{Xe}$ ) and the lighter ( $^{40}\text{Ar}$ ) nuclei with the abrasion-ablation model, it seems that surface energy is approximately right to predict the isotopic distributions of the lighter systems while the heavier systems will be reproduced by including higher excitation energy. From comparison with Sümmerer's parametrization we can see that the nuclear structure, such as the diffuse surface of the nucleus or neutron skin, should be introduced to give a rather broad and lower charged distribution of the pre-fragment. A model, which considers both of these two aspects, will give a better explanation of the isotopic distribution for both the lighter and the heavier projectiles [17].

In conclusion we have measured the isotopic distributions of 44 MeV/nucleon  $^{129}\text{Xe}$  on  $^{90}\text{Zr}$  and  $^{197}\text{Au}$  targets. It can be seen that the reaction process induced by a heavy projectile at intermediate energies is not a pure fragmentation but a complex process including transfer, fragmentation, and dissipation process. Sümmerer's parametrization can be used to predicate the isotopic production cross section for heavier projectile peripheral collisions at intermediate energies. But some large deviations still exist. More experimental data on the isotopic fragmentation distribution are needed in order to make a reliable prediction of the fragmentation cross section for certain isotopes for an estimate of the intensity of secondary radioactive beams.

We would like to acknowledge Dr. X. L. Cheng for her reading of our manuscript. One of the authors (J.F.) wishes to thank Dr. X. Q. Hu for a useful discussion and the hospitality of RIKEN, where part of this work was done. This work was supported partly by the National Nature Science Foundation of China and the Heavy Ion Research Facility of Lanzhou (HIRFL).

- [1] M. Langevin, E. Quiniou, M. Bernas, J. Galin, J. C. Jacmart, F. Naulin, F. Pougheon, R. Anne, C. Detraz, D. Guerreau, D. Guillemaud-Mueller, and A. C. Mueller, *Phys. Lett. B* **150**, 171 (1985).
- [2] J. P. Dufour, R. Del Moral, F. Hubert, D. Jean, M. S. Pravikoff, A. Fleury, A. C. Mueller, K. H. Schmidt, K. Summerer, E. Hanelt, J. Frehaut, M. Beau, and G. Giraudet, *Phys. Lett. B* **206**, 195 (1988).
- [3] D. Guerreau, V. Borrel, D. Jacquet, J. Galin, B. Gatty,

- and X. Tarrago, *Phys. Lett. B* **131**, 293 (1983).
- [4] D. Guillemaud-Mueller *et al.*, *Z. Phys. A* **332**, 189 (1989).
- [5] F. Pougheon, J. C. Jacmart, E. Quiniou, R. Anne, D. Bazin, V. Borrel, J. Galin, D. Guerreau, D. Guillemaud-Mueller, A. C. Mueller, E. Roeckl, M. G. Saint-Laurent, and C. Detraz, *Z. Phys. A* **327**, 17 (1987).
- [6] D. Guerreau, *J. Phys. (Paris) Colloq.* **47**, C4-207 (1986).
- [7] M. G. Saint-Laurent *et al.*, *Phys. Rev. Lett.* **59**, 33 (1987).

- [8] D. Bazin, D. Guerreau, R. Anne, D. Guillemaud-Mueller, A. C. Mueller, and M. G. Saint-Laurent, Nucl. Phys. **A515**, 349 (1990).
- [9] A. Bonesera, M. Di Toro, and C. Gregoire, Nucl. Phys. **A463**, 653 (1987); **A483**, 738 (1987).
- [10] L. Tassun-Got and C. Stephan, Nucl. Phys. **A524**, 121 (1991).
- [11] L. Bianchi, B. Fernandez, J. Gastebios, A. Gillibert, W. Mittig, and J. Barrette, Nucl. Instrum. Methods A **276**, 509 (1989).
- [12] J. Feng, W. Q. Shen, Y. G. Ma, W. L. Zhan, Y. T. Zhu, and Z. Y. Guo, High Energy Phys. Nucl. Phys. **17**, 95 (1993).
- [13] W. Swiatecki (unpublished).
- [14] F. Oliveira, R. Donangelo, and J. O. Rasmussen, Phys. Rev. **19**, 826 (1979).
- [15] D. J. Morrissey, W. R. Marsh, R. J. Otto, W. Loveland, and G. T. Seaborg, Phys. Rev. C **18**, 1267 (1978).
- [16] K. Sümmerer, W. Brüche, D. J. Morrissey, M. Schädel, B. Szweryn, and Yang Weifan, Phys. Rev. C **42**, 2546 (1990).
- [17] J. Feng, W. Q. Shen, and Y. G. Ma (unpublished).